Utilizing Multiple BioMEMS Sensors to Monitor Orthopaedic Strain and Predict Bone Fracture Healing

Jakob G. Wolynski,[1] Conor J. Sutherland,[1] Hilmi Volkan Demir,[2,3] Emre Unal,[3] Akbar Alipour,[4] Christian M. Puttlitz,[1] Kirk C. McGilvray[1]

[1]Department of Mechanical Engineering and School of Biomedical Engineering, Orthopaedic Bioengineering Research Laboratory, Colorado State University, Fort Collins, Colorado, [2]LUMINOUS! Center of Excellence for Semiconductor Lighting and Displays, Microelectronics Division, School of Electrical and Electronics Engineering, and Physics and Applied Physics Division, School of Physical and Mathematical Sciences, Nanyang Technological University, Singapore, [3]Departments of Electrical and Electronics Engineering and Physics, Institute of Materials Science and Nanotechnology (UNAM), Bilkent University, Ankara, Turkey, [4]Division of Cardiology, School of Medicine, Johns Hopkins University, Baltimore, Maryland

Received 14 December 2018; accepted 8 April 2019
Published online in Wiley Online Library (wileyonlinelibrary.com). DOI 10.1002/jor.24325

ABSTRACT: Current diagnostic modalities, such as radiographs or computed tomography, exhibit limited ability to predict the outcome of bone fracture healing. Failed fracture healing after orthopaedic surgical treatments are typically treated by secondary surgery; however, the negative correlation of time between primary and secondary surgeries with resultant health outcome and medical cost accumulation drives the need for improved diagnostic tools. This study describes the simultaneous use of multiple ($n = 5$) implantable flexible substrate wireless microelectromechanical (fsBioMEMS) sensors adhered to an intramedullary nail (IMN) to quantify the biomechanical environment along the length of fracture fixation hardware during simulated healing in ex vivo ovine tibiae. This study further describes the development of an antenna array for interrogation of five fsBioMEMS sensors simultaneously, and quantifies the ability of these sensors to transmit signal through overlaying soft tissues. The ex vivo data indicated significant differences associated with sensor location on the IMN ($p < 0.01$) and fracture state ($p < 0.01$). These data indicate that the fsBioMEMS sensor can serve as a tool to diagnose the current state of fracture healing, and further supports the use of the fsBioMEMS as a means to predict fracture healing due to the known existence of latency between changes in fracture site material properties and radiographic changes. © 2019 Orthopaedic Research Society. Published by Wiley Periodicals, Inc. J Orthop Res 37:1873–1880, 2019

Keywords: microelectromechanical system (MEMS); fracture healing; biomechanics; ovine

During the normal reparative process of orthopaedic fractures, the mechanical stability of the fracture site increases as the injury progresses through the stages of healing.[1–8] It has been shown through the use of wired strain gauges that bone and the healing callus support an increasing fraction of external loads during the healing process, while load fraction is temporally decreased in the implanted surgical hardware.[1,2] In the case of abnormal healing, leading to delayed or non-union, this temporal load sharing profile is significantly altered.[9] Reported incidence rates of delayed and non-union demonstrate large variability,[10–13] reaching values as high as 38%,[13] and are dependent upon the location, severity, and treatment method of the fracture.[10,14–17] In spite of this, it has been shown that implant stability and loading is critically related to bony healing.[1,3–6,18–20] Failed primary operations are often revised via surgical intervention, with the clinical result of these revision procedures being negatively correlated with the time interval between the first and second surgeries due to aggregation of fibrous tissue within the fracture gap.[21] Furthermore, prior studies have suggested a substantial reduction in financial burden when early intervention is implemented to prevent delayed union,[10,22] thus driving the need for early diagnostic modalities with high sensing fidelity/resolution.

Correspondence to: Kirk McGilvray (T: 970-491-1319; F: 970-491-3872; E-mail: kirk.mcgilvray@colostate.edu)

Early fracture healing observation remains a difficult and qualitative process for clinicians,[23–25] which has been identified as an area necessitating diagnostic improvement.[14,26,27] Bone healing is typically monitored through the usage of planar radiographic imaging or manual manipulation of the fracture site. However, physical manipulation is prone to subjective interpretation by the clinician,[28] and radiographs are prone to similar analysis inaccuracies leading to high inter-physician variability.[25–27] Additionally, early radiographic analysis has shown limited success in predicting callus stiffness[29] and likelihood of delayed and non-unions.[26,30] Radiographs are also limited as an early diagnostic tool as they do not indicate healing until sufficient callus calcification, 6–8 weeks post-fracture,[31] thus leading to a 50% probability of correctly predicting union stage.[32] Quantified fracture stiffness, however, elucidates the healing status as much as 2.5 weeks before this information is revealed via radiographic analysis.[8]

There is a current lack of non-invasive diagnostic measures to determine callus strength, a metric which is crucial in diagnosing the state of bone healing and the patient's ability to bear weight.[8,26,33] Previous studies have shown success in the use of sensors to telemetrically quantify construct mechanical environment.[34–40] Use of a single wireless, biocompatible, microelectromechanical system (BioMEMS) sensor has previously utilized the bone-implant load sharing principle to successfully detect statistically significant differences in normal and delayed healing in an ovine animal model as early as 21 days

post-fracture.[9] This study demonstrated that by monitoring hardware strain, via the BioMEMS sensor in an area adjacent to the fracture site, it was possible to detect the healing cascade pathway (i.e., union vs. nonunion) in the critically important early healing time (i.e., prior to radiographic evidence of union vs. nonunion).[9] While the BioMEMS sensor showed effectiveness as a single sensor in orthopaedic plating applications, the rigid substrate of this sensor restricts its clinical applicability to hardware containing regions of flat surface geometry. Furthermore, use of a single sensor limits this technology to providing diagnostic information with regards to the load-sharing between the hardware and healing bone at a single hardware location.

Intra-implant strain on surgical nails and plates differ by over 200%[41,42]; consequently, substantial variations in the location of implant failure have been reported due to stress rising features such as screw holes.[43–45] Despite the vast quantity of literature analyzing the relationships between orthopaedic implant design and fracture healing, there is a lack of definitive consensus on optimum treatment techniques. Use of excessively stiff implants leads to increased rates of non-union, while excessively compliant implants can result in hardware failure.[46] This suggests a potential for an optimum intermediate implant design which could feasibly be patient specific. A better understanding of implant temporal and geometric strain profiles presents a potential tool to improve orthopaedic hardware design; however, to our knowledge, there is no current technology which allows for non-invasive in vivo measurements of implant strain at multiple locations. Accordingly, it is theorized that in vivo measurements of implant strain along the length of orthopaedic implants (i.e., at multiple locations) could have a significant impact on fracture fixation hardware design to substantially improve clinical outcome. To address this need, and the current limitations of the BioMEMS sensor, we have developed an antenna array and a flexible substrate BioMEMS (fsBioMEMS) sensor which allows multiple telemetric sensors to be applied along contoured surfaces of orthopaedic hardware, such as intramedullary nails (IMN) and fracture fixation plates, to simultaneously determine the mechanical environment at multiple discrete locations.

METHODS

A series of increasingly complex in vitro experiments were conducted to characterize a fsBioMEMS sensor-IMN construct. The goal of these experiments was to determine the implant's sensing resolution, effects of soft tissue attenuation, and the sensors' ability to withstand a simulated in vivo environment, with the ultimate experiment simulating a fracture healing scenario in an ovine hind limb.

fsBioMEMS Fabrication

Our group has performed a series of experimental and analytical investigations of increasing complexity upon MEMS-based telemetric measurements of local fracture mechanics by observing shifts in the sensor's resonance response frequency (RRF) using computational models, prototype fabrication, ex vivo simulations, and in vivo animal models.[9,34–40] The current system is composed of a multi-sensor fsBioMEMS sensor-implant construct and an external excitation/receiving apparatus consisting of a multi-antenna array and a network analyzer (Fig. 1). The multi-antenna array is designed with five evenly spaced antennae, allowing for simultaneous excitation/receiving of RRF signals from five independent fsBioMEMS sensors. Each antenna emits an electromagnetic wave with a unique frequency inducing a differential current and associated resonance within each fsBioMEMS sensor. The particular resonance within each sensor is dependent upon its architectural features. Deformation of the sensor's split ring architecture, due to physical loading, induces changes to the sensor's capacitance.[38] Changes in capacitance resulting from external loading produces a shift to the sensor's spectral RRF. The sensor architecture is designed to ensure that the RRF shifts linearly with the sensor's principal strain.[38]

The sensors are fabricated with standard MEMS fabrication methods utilizing a polyimide tape substrate (Kapton HN; DuPont, Wilmington, DE), gold metal layering, and a Si_3N_4 dielectric layer.[34,35] These materials were selected to ensure enhanced sensor performance, while maintaining the requisite biocompatibility.[9] The sensor dimension is a square with 8-mm sides and 0.8-mm thickness (Fig. 1). Sensor and antenna architectures were designed such that each of the five antenna-sensor combinations yield deep and sharp dips in the spectral RRF at sub-GHz frequencies, as described in the proceeding section. The specific fabrication details for the MEMS architecture can be found in previous studies by McGilvray et al.[9] and Melik et al.[36] The only fundamental change within the BioMEMS fabrication process previously described was to replace the rigid silicon substrate with a flexible polyimide substrate.

To create the fsBioMEMS sensor-IMN construct used within this study, five fsBioMEMS sensors were rigidly attached to an 8-mm diameter by 197 mm length IMN (Biomedtrics I-Loc IM Fixator, Whippany, NJ) at evenly spaced distances of 40.64 mm (based upon the placement of sensor 3 at the IMN mid-span) using cyanoacrylate (Locktite, Düsseldorf, Germany) before coating with layers of two-part high tensile strength epoxy (2 Ton Clear Epoxy; Devcon, Danvers, MA) and medical-grade polyurethane (Master Bond, Inc., Hackensack, NJ).

Antenna Array

The use of a multiple antenna array, as opposed to utilizing multiple sensors with varied architecture, has a number of advantages: (i) elimination of the need to trace the implant location of each specific sensor architecture, (ii) utilization of identical sensors, from the same batch, reduces fabrication-induced discrepancies between sensors, (iii) system redesigns can be implemented to the antennae, thus allowing for continued improvements after in vivo sensor implantation. The multi-antenna array was designed to reduce data collection time, minimize cross-talk between sensor-antenna pairs, and to concurrently evaluate all sensors. This is achieved through parallel antenna connection to a two port network analyzer which simultaneously collects the ratio of reflected signal to input signal (reflection coefficient) at each network port (S_{11} and S_{22} parameter data).

Computational simulations were performed to determine prospective antennae designs which were then selected for

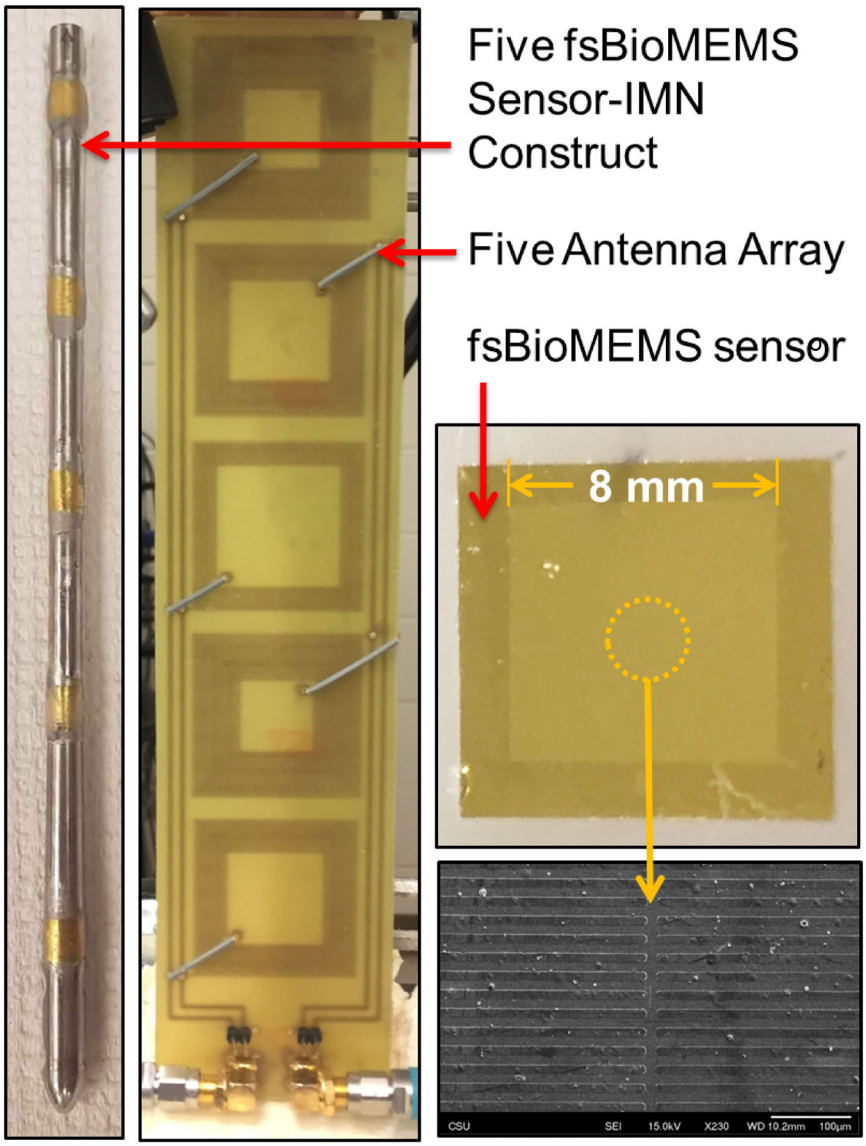

Figure 1. Macro and scanning electron microscopy digital images of a single flexible substrate wireless microelectromechanical (fsBioMEMS) sensor, digital image of the sensor-intramedullary nail (IMN) construct containing five evenly space fsBioMEMS sensors, and a digital image of the five antenna array used for measuring resonant radio frequency (RRF) of the fsBioMEMS sensors. [Color figure can be viewed at wileyonlinelibrary.com]

prototype fabrication (Fig. 2). Benchtop collection of the prototype antennae's RRF data (S_{11} parameter frequency and gain) was performed to determine the operating spectral ranges and quality factors (Q-factor) of the antennae.

Utilization of unique architecture resulted in three feasible antenna designs for prototype analysis. The resulting RRF spectra of these antennae, when coupled to fsBioMEMS sensors, produced discrete, non-overlapping RF spectra (Fig. 3). The Q-factor associated with the antennae demonstrated Q-factor values of 71, 35, and 25 for the v2_f1, v2_f2, and v2_f3 antenna designs; respectively. Parallel deployment of these three architectures while recording two network ports (S_{11} and S_{22}) allows for simultaneous data collection from up to six fsBioMEMS sensors.

Despite each antenna array being designed to contain unique and discrete resonance frequencies, the possibility existed for individual antenna to be effected by multiple sensors; thus, experiments were performed to quantify the relationship between sensor spacing and sensor cross-talk. A sensor was aligned beneath a single antenna while RRF data were collected as a second sensor was moved discrete unidirectional distances from the first sensor (minimum and maximum sensor spacing distances of 10 and 40 mm, respectively). The findings from these experiments were used to produce an antenna array with minimized sensor cross-talk (data given in Supplementary Information).

Tissue Attenuation

In order to ensure in vivo feasibility of the sensor-IMN construct, parametric studies were performed to investigate the effect of soft tissue thickness and/or composition on RRF measurements from the fsBioMEMS sensors.[9] A sensor-IMN construct was placed in a custom loading fixture which allowed for IMN rod bending and unidirectional movement of the antenna array relative to the construct (Fig. 4). Bending was induced (1–4 N-m in 1 N-m increments, $n = 5$ loading cycles per data collection period) by the addition of weights to the cantilever arm while RRF changes in each sensor were measured by the antenna array and network analyzer (R&S ZVB4; Rhode & Schwarz, Munich, Germany). The bending moment was measured with a 6 degree-of-freedom (DOF) load cell (AMTI MC3A-100; AMTI, Watertown, MA). The distance between the antenna

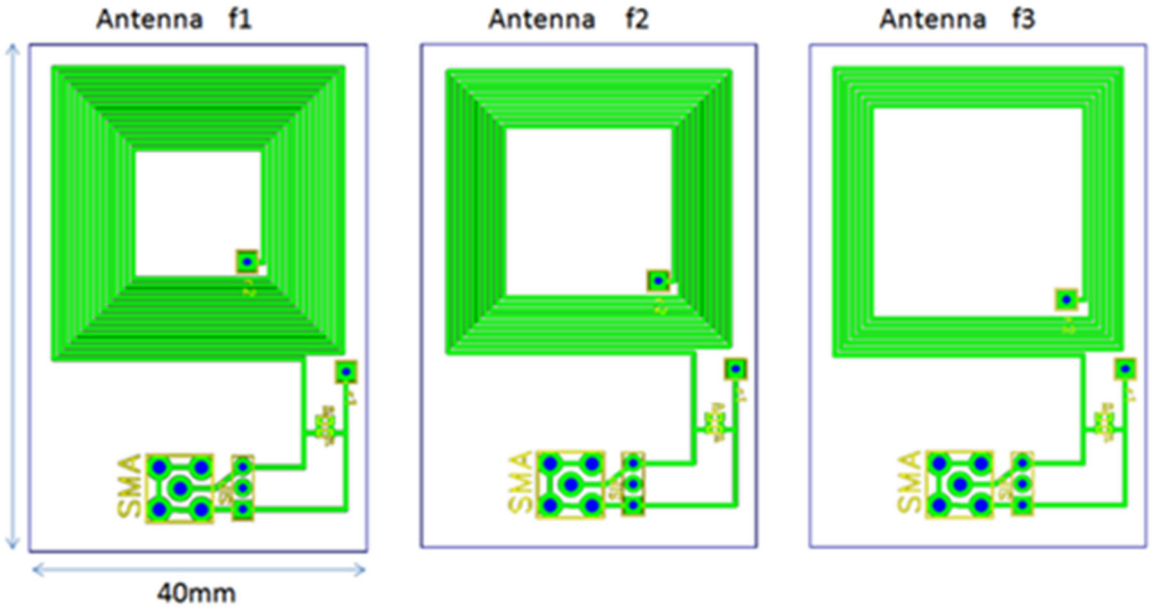

Figure 2. Schematic of the antennae designed to produce non-overlapping response frequency (RF) responses. [Color figure can be viewed at wileyonlinelibrary.com]

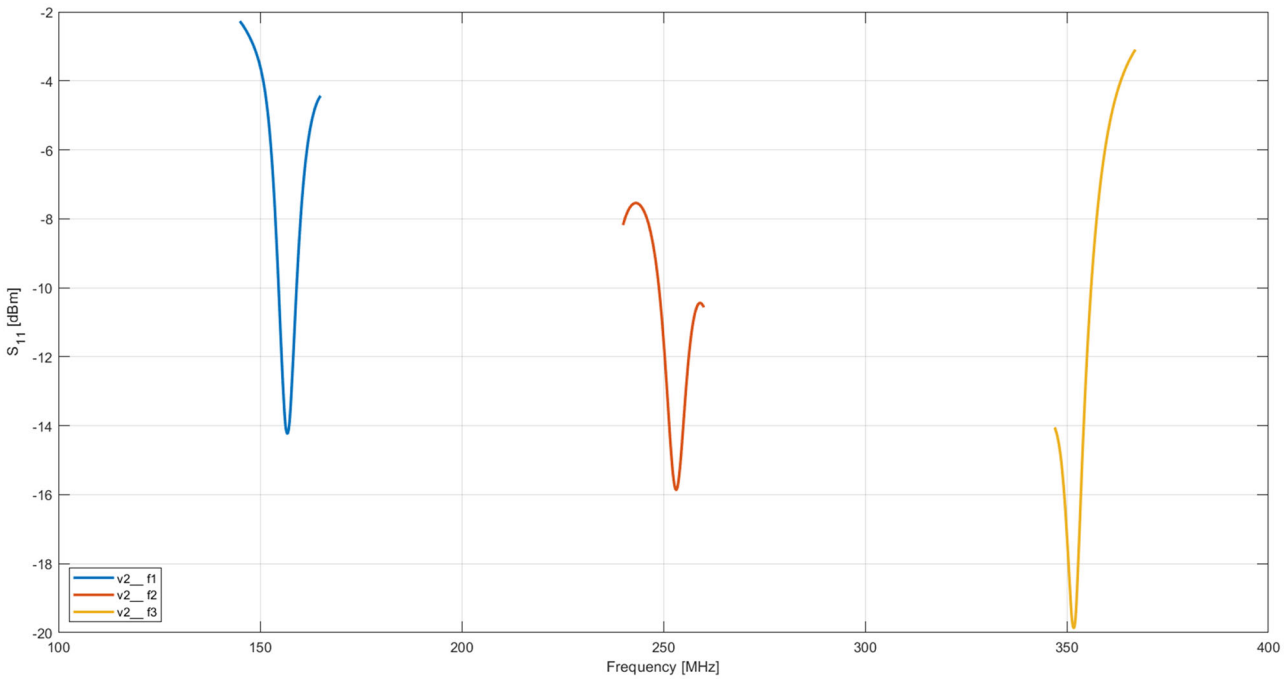

Figure 3. Resonance response frequency (RRF) responses measured for the original and prototype antenna designs. [Color figure can be viewed at wileyonlinelibrary.com]

and IMN-construct was progressively increased as the intervening space was filled with a homogenous composition of cadaveric ovine tissue; this was repeated for multiple tissue types (i.e., muscle, fat, or skin). Tissues for this experiment were collected from unrelated studies. Soft tissue thickness was increased until signal strength was determined to be fully attenuated, as indicated when the average total sensor RRF shift magnitudes diminished to approximately 15% of their initial values (relative to the smallest tissue thickness).

fsBioMEMS Sensor Temporal Sensitivity

To simulate the temporal shift of callus tissue stiffness during normal healing, an ex vivo ovine osteotomy model stabilized by locking IMN was performed.[9] Cadaveric tibae from ovine hind limbs, euthanized for unrelated studies ($n = 9$ hindlimbs), were dissected to remove soft tissue and then fixed with a five sensor-IMN construct. All tibiae were tested using the same sensor-IMN composite to eliminate effects due to differences in sensor placement. Mechanical testing for all tibiae was repeated at three osteotomy states. The

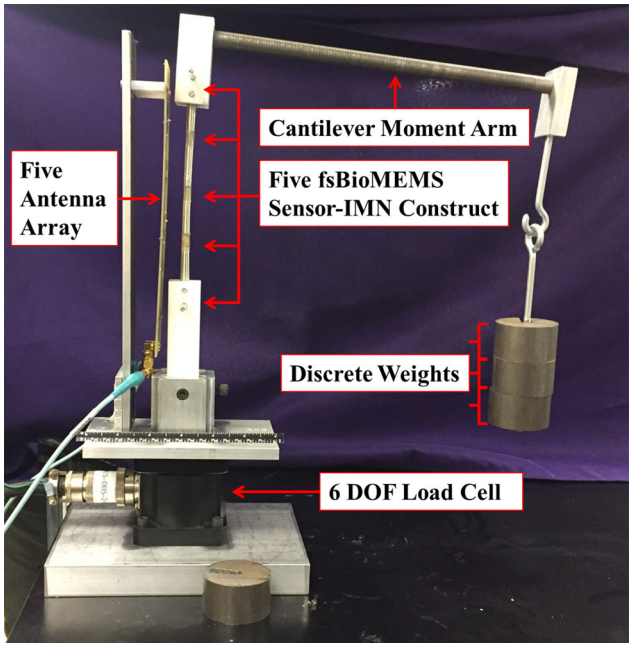

Figure 4. Custom cantilever fixture applying bending moments to a flexible substrate wireless microelectromechanical (fsBioMEMS) sensor-intramedullary nail (IMN) construct while a five antenna array measures the sensors' resonance response frequency (RRF). The fixture design allows for consistent placement of the sensor-IMN construct, relative to the antenna array, during tissue attenuation analysis. [Color figure can be viewed at wileyonlinelibrary.com]

osteotomies were produced by a bone saw cut to reduce cortical bone thickness by half or full thickness near the height of the middle sensor ipsilateral to the bending-induced compression (i.e., opposite the antenna and sensors). In this way, the tibia construct was tested at fully intact, half osteotomy, and full osteotomy states (Fig. 5B).

The ends of each limb were potted in two-part hard cast resin (SmoothCast 321; Smooth-On, Macungie, PA) to ensure proper mechanical fixation. A servo-hydraulic testing system (858 MiniBionix; MTS Systems Corp., Eden Prairie, MN) was used to apply compressive loads (100–700 N in 100 N increments; $n = 5$ cyclic tests per sample per fracture state) to the potted construct while measuring the RRF spectrum of each sensor using the antenna array and network analyzer (Fig. 5). The testing set-up was designed to apply combined compression and bending loading, while further allowing for consistent placement of the antenna array relative to the tibia across all fracture states. Sensor sensitivity was calculated as the mean slope of a linear fit trend line to each cycle's load-RRF data.

Statistical Analyses

All data were analyzed for normality before statistical differences were determined using a one-way analysis of variance (ANOVA). When statistical differences between groups were indicated by the ANOVA, specific statistical significances were determined by a post hoc Tukey test (Minitab, State College, PA). Non-normally distributed data was evaluated for statistical significance using a Kruskal–Wallis test and post hoc Dunn's test. $p < 0.05$ was considered statistically significant.

RESULTS

Tissue Attenuation

Signal attenuation experiments demonstrated that RRF signal changes could be measured through as much as 90 mm of muscle, 50 mm of fat, or 30 mm of skin. Measurements of signal through an unobstructed air gap established a loss of measurable RRF signal change after 10 mm (Fig. 6).

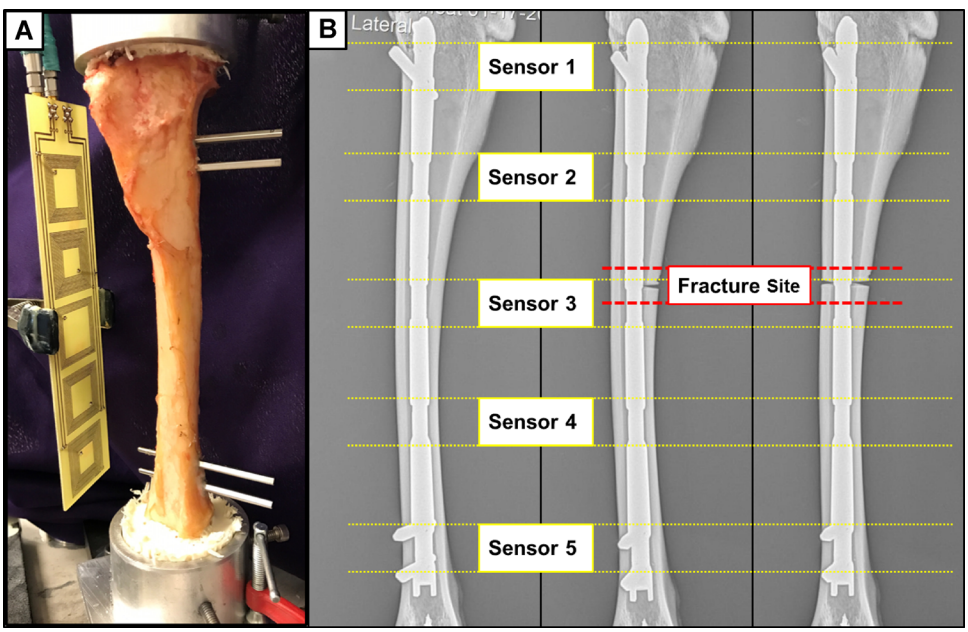

Figure 5. (A) Dissected ovine tibia, fixed via flexible substrate wireless microelectromechanical (fsBioMEMS) sensor-intramedullary nail (IMN) construct, undergoing complex loading (compression and bending) while a five antenna array measures the resonance response frequency (RRF) of the five fsBioMEMS sensors. (B) Radiographs demonstrating the five fsBioMEMS sensor locations and osteotomy states used to simulate the temporally increasing bone stiffness of a healing fracture: fully intact, half osteotomy, full osteotomy (from left to right). [Color figure can be viewed at wileyonlinelibrary.com]

fsBioMEMS Sensor Temporal Sensitivity

An ex vivo ovine tibia fracture model, surgically stabilized by sensor-IMN constructs, indicated it was possible to correlate changes in sensor RRF response to construct loading under compression-bending complex loads. When grouping all samples, the average sensor sensitivities decreased as the amount of bone at the osteotomy site increased, with the exception of sensor 5 from the full osteotomy to half osteotomy models which increased from 81.5 to 83.5 Hz/N, an increase of 2.4% (Fig. 7A). For sensors 1–4, the sensitivities from the full osteotomy to half osteotomy states decreased by 44.8%, 35.4%, 34.4%, and 50.8%; respectively (Fig. 7A). Similarly, sensitivities from half osteotomy to fully intact states decreased by 36.3%, 32.5%, 39.5%, 45.7%, and 25.0% for sensors 1–5, respectively (Fig. 7A).

An ANOVA statistical test ($\alpha = 0.05$) of the compiled sample averages, indicated statistically significant differences associated with sensor location ($p = 0.001$) and fracture state ($p = 0.004$). Tukey pairwise comparisons ($\alpha = 0.05$) specified the average sensitivity of sensor 1 as significantly different than sensors 3, 4, and 5 ($p = 0.034$, $p = 0.001$, and $p = 0.017$, respectively), while the full osteotomy state showed statistically significant differences from the half osteotomy and intact states ($p = 0.044$ and $p = 0.004$, respectively). The large variability in grouped sensor sensitivities (Fig. 7A) was not indicative of the sensitivities observed within single samples (Fig. 7B).

DISCUSSION

A multi-antenna array was developed which produces antenna-sensor pair RRF responses in discrete, non-overlapping spectral ranges. By utilizing parallel antenna connectivity, and simultaneous measurement of S_{11} (from sensors 1, 3, and 5) and S_{22} (from sensors 2 and 4) data, this array allowed for concurrent measurement of RRF behavior of five antenna-sensor pairs. In addition to increasing the number of fsBioMEMS sensors which can be placed on a single implant, this measurement technique has the auxiliary benefit of reducing the data collection period by 50% without reduction of resolution. The spectra of the new antenna design feature substantially increased Q-factors (relative to the original antenna design) thus allowing for data noise reduction. Enhanced Q-factors are the result of deep and sharp RRF peaks, which has the added benefit of decreasing the total frequency range which must be analyzed for a five-sensor construct. Reducing this range decreases the burden on the network analyzer, enabling further increased data acquisition times which more closely approach real-time measurement.

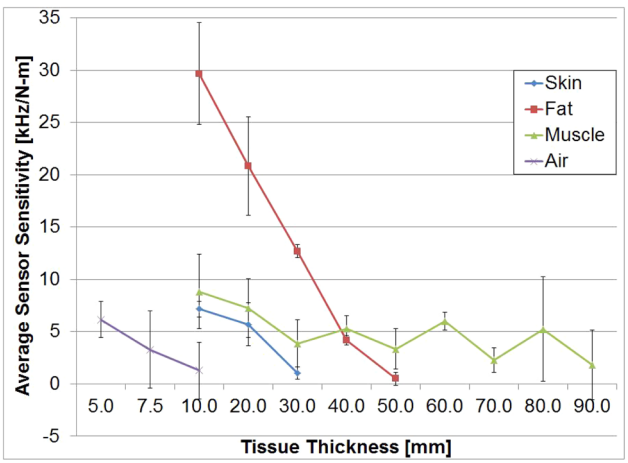

Figure 6. Comparison of the effects of intervening ovine cadaveric tissue type and thickness on sensor sensitivity. Sensor sensitivity through 30 mm of skin differed significantly from 10 mm ($p = 0.002$) and 20 mm of skin ($p = 0.028$). Within fat, sensitivity at 10-mm thickness was significantly different from 40 mm ($p = 0.001$) and 50 mm ($p < 0.001$), and 20-mm thickness exhibited significantly higher sensitivity than 50 mm ($p = 0.001$). Sensitivity through 10 mm of muscle differed significantly from 70 mm ($p = 0.015$) and 90 mm of muscle ($p = 0.009$). [Color figure can be viewed at wileyonlinelibrary.com]

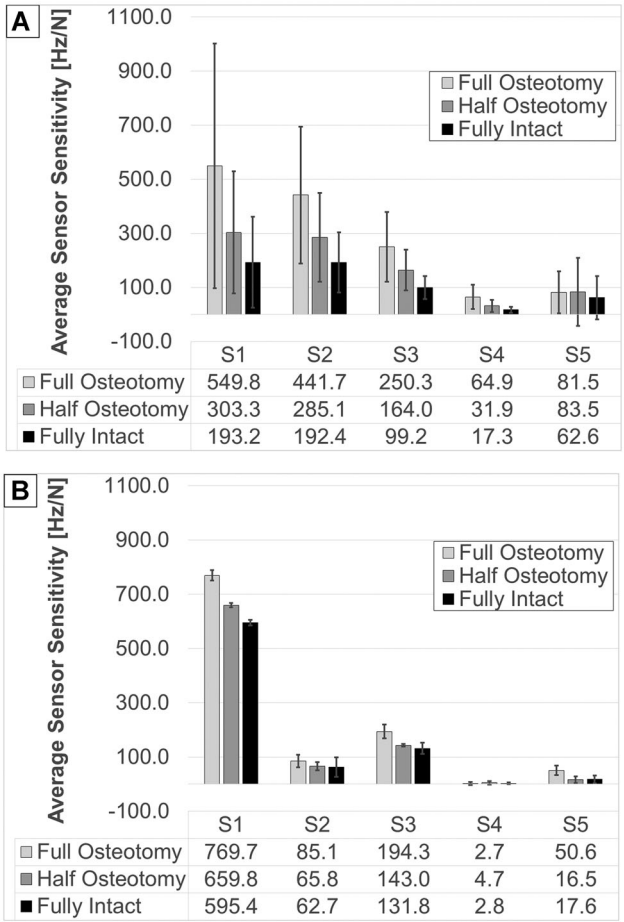

Figure 7. (A) Average compiled ($n = 9$) sensor sensitivities for a five flexible substrate wireless microelectromechanical (fsBioMEMS) sensor-intramedullary nail (IMN) construct during ex vivo simulated bone healing of ovine tibia. The sensors are numbered from proximal (S1) to distal (S5), with S3 located at the IMN mid-span. Based upon an analysis of variance (ANOVA) with Tukey's pairwise comparisons ($\alpha = 0.05$), the full osteotomy state differs significantly from the half osteotomy and intact states ($p = 0.044$ and $p = 0.004$, respectively) and the mean sensitivity of sensor 1 differs significantly from sensors 3, 4, and 5 ($p = 0.034$, $p = 0.001$, and $p = 0.017$, respectively). (B) Average sensor sensitivities for a single ovine tibia ($n = 5$ cycles per fracture state).

Analysis of cross-talk indicated deleterious effects induced by the presence of multiple sensors within close proximity to a single antenna. These effects diminished considerably once the second sensor was displaced outside of the projection area of a given antenna. Cross-talk was further observed between two adjacent antennae. Once again, effects were greatest while the antennae projection areas overlapped. Cross-talk effects appeared to be exacerbated in instances of the antennae having similar operating frequencies. The results of this analysis were utilized to develop an antenna array which focused upon the geometric and spectral relationship between adjacent antenna, with specific regards to eliminating overlap in the projection areas and maximizing the difference in operating frequencies.

Sensor repeatability and tissue attenuation data indicated plausibility in the ability to measure RRF spectra of the sensor-IMN construct in vivo; however, the performance of this diagnostic measure could foreseeably vary among certain patients where excessive amounts of tissue intervene between the skin and implant. Tissue attenuation data further highlighted the importance of close proximity between the tissue and antenna during data acquisition due to the high degree of signal attenuation within air.

Measurements from the present study suggest a decrease in load share experienced by implant hardware as fracture stiffness increases. Previous studies have exhibited similar trends through a variety of testing methods including the use of wired external fixators in humans[7] and sheep,[2] wired strain gauges on fixation plates in sheep,[1] and telemetric assessment of femoral IMNs in humans.[47] These findings are further supported by a previous study by our group, through the use of a single BioMEMS sensor on fixation plates in sheep, which found decreasing implant strain throughout the healing process. Differences in healing types were detectable with this method during early phases of healing.[9] The data of the present study advocate that multi-sensor fsBioMEMS constructs contain the same diagnostic abilities, with the addition of applicability towards contoured implants at multiple locations.

Current clinical early diagnostic tools are limited in their ability to predict the course of fracture healing.[26–30,32,33] Healing is typically monitored through the use of temporal radiographs after surgical intervention. However, radiographic imaging suffers from a number of disadvantages, including limited fidelity and patient exposure to ionizing radiation.[33] When interpreted by experienced clinicians, there is a great deal of inter-observer variability in estimating the progress of healing.[25–27] Furthermore, early radiographs have demonstrated an inadequate ability to properly predict the course of healing.[26,29,30,32] Previous studies have aimed to decrease the subjectivity of this diagnostic modality through the use of scoring methods[48] and automated image processing algorithms,[49] but these neglect to address the low temporal fidelity of radiographs. Prior studies have established the appearance of calcified tissue (during secondary bone formation) to present radiographically several weeks after healing is indicated by quantifiable changes in the temporal mechanical properties of the periosteal callus.[8,47] Moreover, radiographic imaging presents little temporal changes in the case of primary bone healing, where healing is slow and no periosteal callus is formed.[14] The need for quantification of the mechanical environment of the fracture implant is motivated by increased temporal fidelity (relative to standard imaging modalities) and the associated dependency between implant loading and fracture healing.[1,5]

The use of fsBioMEMS sensors present clinical potential due to a number of advantageous features, including: their small and flexible nature which allows for efficacious placement on orthopaedic hardware, inductive power allowing for long-term use without the need for power source implantation, and wireless transmission allowing for non-invasive measurements. An added benefit is derived through the use of sensors on multiple locations of orthopaedic implants. Improvements to the sensing technology to obviate differences in inter-sensor measurement sensitivities would allow for direct comparison of strain at several locations, thus creating a temporal strain profile along the length of the implant. These data could be leveraged as a development tool for the creation of orthopaedic hardware in order to optimize the mechanical environment for bone healing.

AUTHORS' CONTRIBUTION

J.G.W., C.J.S., H.V.D., E.U., A.A., C.M.P., and K.C.M. were involved in the study design, data collection, data interpretation, and preparation of the manuscript. All authors have read and approved the manuscript.

ACKNOWLEDGEMENTS

Funding for this project came from the National Institute of Health—NIAMS (R01AR069734-01—"Early Detection and Prediction of Complex Bone Fracture Healing"). Demir and Puttlitz are the founding and managing partners of Innovative In Vivo Sensing, LLC, a corporate entity, which holds all intellectual property rights of the BioMEMS technology presented in this manuscript.

REFERENCES

1. Stoffel K, Klaue K, Perren SM. 2000. Functional load of plates in fracture fixation in vivo and its correlate in bone healing. Injury 31:S-b37–S-b50.
2. Grasa J, Gomez-Benito MJ, Gonzalez-Torres LA, et al. 2010. Monitoring in vivo load transmission through an external fixator. Ann Biomed Eng 38:605–612.
3. Claes LE, Wilke HJ, Augat P, et al. 1995. Effect of dynamization on gap healing of diaphyseal fractures under external fixation. Clin Biomech (Bristol, Avon) 10:227–234.
4. Claes LE, Heigele CA. 1999. Magnitudes of local stress and strain along bony surfaces predict the course and type of fracture healing. J Biomech 32:255–266.
5. Claes LE, Heigele CA, Neidlinger-Wilke C, et al. 1998. Effects of mechanical factors on the fracture healing process. Clin Orthop Relat Res, S137–S147.

6. Gadomski BC, McGilvray KC, Easley JT, et al. 2014. Partial gravity unloading inhibits bone healing responses in a large animal model. J Biomech 47:2836–2842.
7. Claes LE, Cunningham JL. 2009. Monitoring the mechanical properties of healing bone. Clin Orthop Relat Res 467:1964–1971.
8. Claes L, Grass R, Schmickal T, et al. 2002. Monitoring and healing analysis of 100 tibial shaft fractures. Langenbecks Arch Surg 387:146–152.
9. McGilvray KC, Unal E, Troyer KL, et al. 2015. Implantable microelectromechanical sensors for diagnostic monitoring and post-surgical prediction of bone fracture healing. J Orthop Res 33:1439–1446.
10. Heckman JD, Sarasohn-Kahn J. 1997. The economics of treating tibia fractures. The cost of delayed unions. Bull Hosp Jt Dis 56:63–72.
11. Weissman SL, Herold HZ, Engelberg M. 1966. Fractures of the middle two-thirds of the tibial shaft. J Bone Joint Surg Am 48:257–267.
12. Nicoll EA. 1964. Fractures of the tibial shaft. A survey of 705 cases. J Bone Joint Surg Br 46:373–387.
13. Jackson RW, Macnab I. 1959. Fractures of the shaft of the tibia; a clinical and experimental study. Am J Surg 97:543–557.
14. Hak DJ, Fitzpatrick D, Bishop JA, et al. 2014. Delayed union and nonunions: epidemiology, clinical issues, and financial aspects. Injury 45:S3–S7.
15. Tay WH, de Steiger R, Richardson M, et al. 2014. Health outcomes of delayed union and nonunion of femoral and tibial shaft fractures. Injury 45:1653–1658.
16. Tzioupis C, Giannoudis PV. 2007. Prevalence of long-bone non-unions. Injury 38:S3–S9.
17. Dickson K, Katzman S, Delgado E, et al. 1994. Delayed unions and nonunions of open tibial fractures. Correlation with arteriography results. Clin Orthop Relat Res 302:189–193.
18. Miclau T, Lu C, Thompson Z, et al. 2007. Effects of delayed stabilization on fracture healing. J Orthop Res 25:1552–1558.
19. Goodship AE, Kenwright J. 1985. The influence of induced micromovement upon the healing of experimental tibial fractures. J Bone Joint Surg Br 67:650–655.
20. Uhthoff HK, Poitras P, Backman DS. 2006. Internal plate fixation of fractures: short history and recent developments. J Orthop Sci 11:118–126.
21. Garcia P, Holstein JH, Maier S, et al. 2008. Development of a reliable non-union model in mice. J Surg Res 147:84–91.
22. Kanakaris NK, Giannoudis PV. 2007. The health economics of the treatment of long-bone non-unions. Injury 38:S77–S84.
23. Nicholls PJ, Berg E, Blivern FE, Jr., et al. 1979. X-ray diagnosis of healing fractures in rabbits. Clin Orthop Relat Res 142:234–236.
24. Whelan DB, Bhandari M, McKee MD, et al. 2002. Interobserver and intraobserver variation in the assessment of the healing of tibial fractures after intramedullary fixation. J Bone Joint Surg Br 84:15–18.
25. Bhandari M, Guyatt GH, Swiontkowski MF, et al. 2002. A lack of consensus in the assessment of fracture healing among orthopaedic surgeons. J Orthop Trauma 16:562–566.
26. McClelland D, Thomas PB, Bancroft G, et al. 2007. Fracture healing assessment comparing stiffness measurements using radiographs. Clin Orthop Relat Res 457:214–219.
27. Corrales LA, Morshed S, Bhandari M, et al. 2008. Variability in the assessment of fracture-healing in orthopaedic trauma studies. J Bone Joint Surg Am 90:1862–1868.
28. Webb J, Herling G, Gardner T, et al. 1996. Manual assessment of fracture stiffness. Injury 27:319–320.
29. Panjabi MM, Walter SD, Karuda M, et al. 1985. Correlations of radiographic analysis of healing fractures with strength: a statistical analysis of experimental osteotomies. J Orthop Res 3:212–218.
30. Davis BJ, Roberts PJ, Moorcroft CI, et al. 2004. Reliability of radiographs in defining union of internally fixed fractures. Injury 35:557–561.
31. Young JW, et al. 1990. Sonographic evaluation of bone production at the distraction site in Ilizarov limb-lengthening procedures. AJR Am J Roentgenol 154:125–128.
32. Hammer RR, Hammerby S, Lindholm B. 1985. Accuracy of radiologic assessment of tibial shaft fracture union in humans. Clin Orthop Relat Res 199:233–238.
33. Augat P, Morgan EF, Lujan TJ, et al. 2014. Imaging techniques for the assessment of fracture repair. Injury 45:S16–S22.
34. Melik R, Perkgoz NK, Unal E, et al. 2008. Bio-implantable passive on-chip RF-MEMS strain sensing resonators for orthopaedic applications. J Micromech Microeng 18:115017.
35. Melik R, Unal E, Perkgoz NK, et al. 2010. Nested metamaterials for wireless strain sensing. IEEE J Selectd Top Quantum Electron 16:450–458.
36. Melik R, Unal E, Perkgoz NK, et al. 2009. Circular high-Q resonating isotropic strain sensors with large shift of resonance frequency under stress. Sensors (Basel) 9:9444–9451.
37. Melik R, Unal E, Perkgoz NK, et al. 2010. Metamaterial based telemetric strain sensing in different materials. Opt Express 18:5000–5007.
38. Melik R, Unal E, Perkgoz NK, et al. 2009. Flexible metamaterials for wireless strain sensing. Appl Phys Lett 95:181105.
39. Melik R, Unal E, Perkgoz NK, et al. 2009. Metamaterial-based wireless strain sensors. Appl Phys Lett 95:011106.
40. Melik R, Unal E, Perkgoz NK, et al. 2011. RF-MEMS load sensors with enhanced Q-factor and sensitivity in a suspended architecture. Microelectron Eng 88:247–253.
41. Hak DJ, Neiman R, Hazelwood S. 2010. Biomechanical strain analysis of the proximal femur following retrograde intramedullary nailing. Curr Orthop Pract 21:385–389.
42. Montanini R, Filardi V. 2010. In vitro biomechanical evaluation of antegrade femoral nailing at early and late postoperative stages. Med Eng Phys 32:889–897.
43. Kregor PJ, Stannard JA, Zlowodski M, et al. 2004. Treatment of distal femur fractures using the less invasive stabilization system: surgical experience and early clinical results in 103 fractures. J Orthop Trauma 18:509–520.
44. Firoozabadi R, McDonald E, Nguyen TQ, et al. 2012. Does plugging unused combination screw holes improve the fatigue life of fixation with locking plates in comminuted supracondylar fractures of the femur? J Bone Joint Surg Br 94:241–248.
45. Vallier HA, Hennessey TA, Sontich JK, et al. 2006. Failure of LCP condylar plate fixation in the distal part of the femur. A report of six cases. J Bone Joint Surg Am 88:846–853.
46. Henderson CE, Kuhl LL, Fitzpatrick DC, et al. 2011. Locking plates for distal femur fractures: is there a problem with fracture healing? J Orthop Trauma 25:S8–S14.
47. Seide K, Aljudaibi M, Weinrish N, et al. 2012. Telemetric assessment of bone healing with an instrumented internal fixator: a preliminary study. J Bone Joint Surg Br 94:398–404.
48. Whelan DB, Bhandari M, McKee MD, et al. 2010. Development of the radiographic union score for tibial fractures for the assessment of tibial fracture healing after intramedullary fixation. J Trauma 68:629–632.
49. Lujan TJ, Madey SM, Fitzpatrick DC, et al. 2010. A computational technique to measure fracture callus in radiographs. J Biomech 43:792–795.

SUPPORTING INFORMATION

Additional supporting information may be found in the online version of this article.